A fast and precise tool for multi-layer planar coil self-inductance calculation

Andreia Raquel S. Faria
Industrial Electronic Engineering Department
University of Minho
Guimarães, Portugal
id6904@uminho.pt

Luís Silvino Marques
Centre of Physics
Porto and Minho Universities
Braga, Portugal
lsam@fisica.uminho.pt

Carlos Ferreira
Industrial Electronic Engineering Department
University of Minho
Guimarães, Portugal
id6642@alunos.uminho.pt

Filipe Serra Alves
Microfabrication and Exploratory Nanotechnology
International Iberian Nanotechnology Laboratory
Braga, Portugal
filipe.alves@inl.int

Jorge Miguel N. S. Cabral
Industrial Electronic Engineering Department
University of Minho
Guimarães, Portugal
jcabral@dei.uminho.pt

***Abstract*—A tool that allows for a fast and precise analytical calculation of multi-layer planar coils self-inductance, without any geometry limitation is proposed here. For competitive markets, the time to develop a product is a critical aspect. The process of designing and simulating planar coils to achieve reliable results is commonly limited on accuracy and or geometry, or are too time-consuming and expensive, thus a tool to speed up this design process is desired. The model is based on Grover equations, valid for any geometry. The validation of the tool was performed through the comparison with experimental measurements, FEM simulations, and the main analytical methods usually used in literature, with errors registered to be below 2.5%, when compared to FEM simulations. This model offers a new approach to the calculation of the self-inductance of planar coils of several layers that combines precision, speed, independence of geometry, easy interaction, and no need for extra resources.**

***Index Terms*—planar coil, auto-inductance, versatile tool**

I. Introduction

Over the years, it has been perceptible the growth of solutions based on technologies using planar coils [1], [2]. Due to its fabrication and operating characteristics, planar coils offer solutions with a lower weight, better mechanical stability, and volume efficiency, when compared to solenoids, enabling its use in a wide range of applications [2], [3]. Additionally, since planar coils can be printed on traditional circuit boards (PCB) or on flexible materials, a highly repeatable, predictable, and economically efficient production can be achieved, facilitating assembly and integration processes [4]–[6]. The combination of this production method with the high reliability of inductive based technologies, results in the creation of solutions that offer robustness, durability, good thermal behavior, flexible design, high replication capability, for applications in wet and harsh conditions, like oil and dust [7], [8]. Due to its characteristics and functionalities, PCB based planar coils meet many of the requirements imposed by competitive industries, such as automotive, healthcare, robotics, electronics, from low-power to high-power applications [9]–[11]. In the automotive industry, planar coils have been widely used, for example in Electric Vehicles (EVs) [12], through the integration of wireless power transfer (WPT) systems. The evolution of these systems will contribute to the improvement of the dynamic wireless charging (DWC) process, mitigating some of the major barriers for EVs adoption related to the management of stored energy, battery capacity, charging time, and the high costs associated with it [12]. In the medical devices industry, planar coils have also been used to charge implantable devices [9], [13]. This allows not only to reduce the size of the implantable devices, since smaller batteries are needed, but also reduced the need for replacement surgeries and consequently the risk of patient infections or damage to organs or muscle tissues. Planar coils are also used in different sensing applications, due to their ability to satisfy the constraints related to the device's size, the manufacturing costs, and hostile working conditions. Currently, there are already displacement and angular position sensors in the market that integrate planar coils in their transduction mechanism, such as the eddy current effect or inductive coupling [2], [14], [15], like the magnet-free IPS2200 inductive position sensors produced by Renesas company [16].

Considering the strong interest of several industries in planar coil technology, and the huge competitiveness of the markets, the development cycle of new devices has to be shortened, to keep up with this competitiveness [2]. The design and optimization of planar coils is a complex, costly and time consuming process, usually based on finite- element modeling (FEM) methods and experimental measurements [17]–[19]. Fast, closed form analytical methods can also be found in the literature [1], [8], [20]–[26] for coil optimization, however, these methods are limited to the calculation of the self-inductance of regular coils with specific geometries.

In this work an analytical tool to calculate the self-inductance of generic multi-layer planar coils is proposed, combining precision, versatility, and speed. The main goal is

to improve and simplify the design process of planar coils, with minimal computational resources, allowing the analysis of how different parameters (number of turns, space between turns, turns width, the number of segments per turn, inner and outer diameters) influence the coil's inductance. The following sections present and validate the analytical model proposed. Section II details the proposed analytical calculation method of planar coils, while section III validates the proposed model through the comparison with FEM simulations, and experimental measurements. In order to have a more complete validation, different coil geometries and dimensions were analysed. In section IV, the main conclusions of the model validation are drawn and it's effectiveness is discussed.

II. Methods: Analytical Model for Planar Coil Inductance Calculation

The main goal of the proposed model is to be able to calculate a coil self-inductance, regardless of its geometry or number of layers. The coil is treated as a group of connected segments, where it's inductance is calculated through the sum of the self-inductance of every conductor segment, plus the mutual inductance between each of the segments, using Grover equations [27], [28].

Considering the coil's example of Fig. 1, its inductance, L_T, can be calculated using:

$$L_T = L_0 + M_+ - M_-$$

$$\begin{aligned} L_0 = {} & L_{self1} + L_{self2} + L_{self3} + L_{self4} + L_{self5} \\ & + L_{self6} + L_{self7} + L_{self8} + L_{self9} \\ & + L_{self10} + L_{self11} + L_{self12} \end{aligned}$$

$$\begin{aligned} M_+ = {} & 2(M_{1,5} + M_{2,6} + M_{3,7} + M_{4,8} + \\ & + M_{5,9} + M_{6,10} + M_{7,11} + M_{8,12}) \end{aligned}$$

$$\begin{aligned} M_- = {} & 2(M_{1,7} + M_{1,3} + M_{1,11} + M_{5,7} + M_{5,3} + M_{5,11} \\ & + M_{9,7} + M_{9,3} + M_{9,11} + M_{2,8} + M_{2,4} + M_{2,12} \\ & + M_{6,8} + M_{6,4} + M_{6,12} + M_{10,8} + M_{10,4} + M_{10,12}) \end{aligned} \quad (1)$$

where L_T is the total inductance of the coil; L_{selfi} is the self-inductance of straight conductor i; M_+ is the mutual inductance of segments with currents in the same direction; and M_- is the total mutual inductance of segments with currents in opposite directions. The self-inductance of a conductor with a rectangular cross-section can be determined by:

$$L_{self} = 0.002l(\ln(\frac{2l}{w+t}) + 0.50049 + \frac{w+t}{3l}) \quad (2)$$

where l (cm) is the conductor length; w (cm) the wire width; and t (cm) its thickness. The mutual inductance between parallel segments (Fig. 2) can be calculated through [27]:

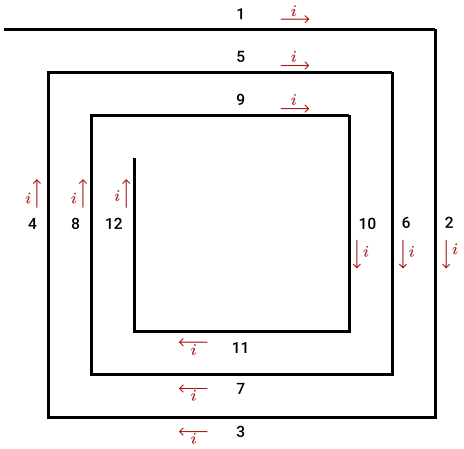

Fig. 1. Square planar coil with three turns.

$$\begin{aligned} M = {} & \frac{\mu_0}{4\times\pi}[\alpha \sinh^{-1}\frac{\alpha}{d} - \beta \sinh^{-1}\frac{\beta}{d} - \gamma \sinh^{-1}\frac{\gamma}{d} \\ & + \delta \sinh^{-1}\frac{\delta}{d} - \sqrt{\alpha^2+d^2} + \sqrt{\beta^2+d^2} \\ & + \sqrt{\gamma^2+d^2} - \sqrt{\delta^2+d^2}] \end{aligned} \quad (3)$$

where $\alpha = l + m + \delta$, $\beta = l + \delta$, and $\gamma = m + \delta$, being l and m the length of the segments in cm. In case the segments overlap (Fig. 2B), it becomes $\alpha = l + m - \delta$, $\beta = l - \delta$, and $\gamma = m - \delta$.

For two nonparallel segments their mutual inductance can be determined by:

$$\begin{aligned} M = {} & \frac{\mu_0}{2\times\pi}\cos\theta[(\mu+l)\tanh^{-1}\frac{m}{R_1+R_2} \\ & + (v+m)\tanh^{-1}\frac{l}{R_1+R_4} - \mu\tanh^{-1}\frac{m}{R_3+R_4} \\ & - v\tanh^{-1}\frac{l}{R_2+R_3}] \end{aligned} \quad (4)$$

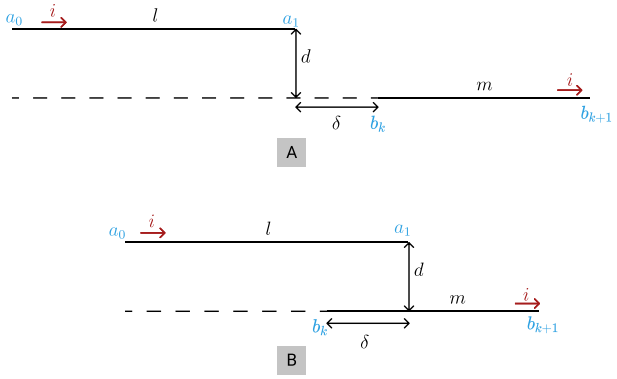

Fig. 2. Mutual Inductance's general case of two parallel filaments, A: Two filaments non overlapped; B: Two filaments overlapped.

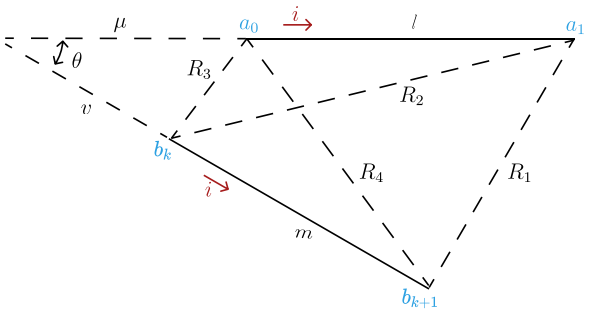

Fig. 3. Mutual Inductance's general case of two nonparallel filaments.

$$2\cos\theta = \frac{\alpha^2}{lm}\alpha^2 = {R_4}^2 - {R_3}^2 + {R_2}^2 - {R_1}^2 \tag{5}$$

$$\mu = \frac{[2m^2({R_2}^2 - {R_3}^2 - l^2) + \alpha^2({R_4}^2 - {R_3}^2 - m^2)]l}{4l^2m^2 - \alpha^4} \tag{6}$$

$$v = \frac{[2l^2({R_4}^2 - R_3^2 - m^2) + \alpha^2({R_2}^2 - {R_3}^2 - l^2)]m}{4l^2m^2 - \alpha^4} \tag{7}$$

$$\begin{aligned} {R_1}^2 &= (\mu + l)^2 + (v + m)^2 - 2(\mu + l)(v + m)\cos\theta \\ {R_2}^2 &= (\mu + l)^2 + v^2 - 2v(\mu + l)\cos\theta \\ {R_3}^2 &= \mu^2 + v^2 - 2\mu v\cos\theta \\ {R_4}^2 &= \mu^2 + (v + m)^2 - 2\mu(v + m)\cos\theta \end{aligned} \tag{8}$$

with l, m representing the length of the segments in cm, θ the angle between segments, and R_1, R_2, R_3, and R_4 the distance between their terminals (Fig. 3).

III. Results and Discussions

The proposed model will be validated by comparing the results with well-known analytical formulas [29] (for the geometries to which they are applicable), considering single and multi-layer planar coils [20], as well as with FEM simulations and experimental measurements. Apart from the different number of layers, other coil's parameters have been testes during validation, such as, line width (w), space between turns (s), number of turns (N), and number of segments per turn (N_s). As the typical analytical formulas are valid just for coils with 4, 6, and 8 segments per turn, the coils with 10 and 12 segments in each turn are validated only with FEM results and experimental measurements. In what concerns w and s, considering the limitations of the Current Sheet Approximation formula, the same values were considered for both parameters ($s = w$), specifically $0.15mm$ and $0.10mm$. It was also taken into account that, according to [20], the coupling factor expression required for multi-layer calculations is only valid for coils with 5 to 20 turns with a distance between layers from $0.75mm$ to $2.0mm$. All the settings used in the different simulation cases are summarized in Table I.

TABLE I
Summary of the different simulation groups.

(A) Coils of 1 layer

L_0*	$w = s$	N
0.3	0.15	4 10
1.3	0.10 0.15	8 10

(B) Coils of 2 layers

L_0*	$w = s$	N
1.3	$0.15mm$	10

* L_0: inner segment's length, w: wire's with, s: space between turns, N: number of turns.

A. Analytical Models VS FEM Model

In this section, a comparison between the coil's inductance values obtained with the proposed model, with the analytical formulas, and the FEM simulations, used as the reference values, is performed .

Fig. 4$A-E$ and 5 show the example geometries for 1 and 2-layer coil , respectively, used in this analysis. As referred before, due to the applicability limitations of the traditional analytical formulas, they were only applied to layouts $A-C$ from Fig. 4 and 5.

The finite element simulations were performed in Ansys software as a magnetic Magnetic problem, specifically the Eddy current mode. It was also studied as a Magnetostatic problem, but was not considered to relevant for this study, considering the experimental validation to be performed. The FEM model considers an air-box with a side dimension of five times the coil outer diameter, as shown in Fig. 6A for a 1-layer square coil example, and Fig. 7 for a 2-layer square coil example. A test current of $1mA$ has been used in both models, with the solver frequency selected to be $1MHz$. The

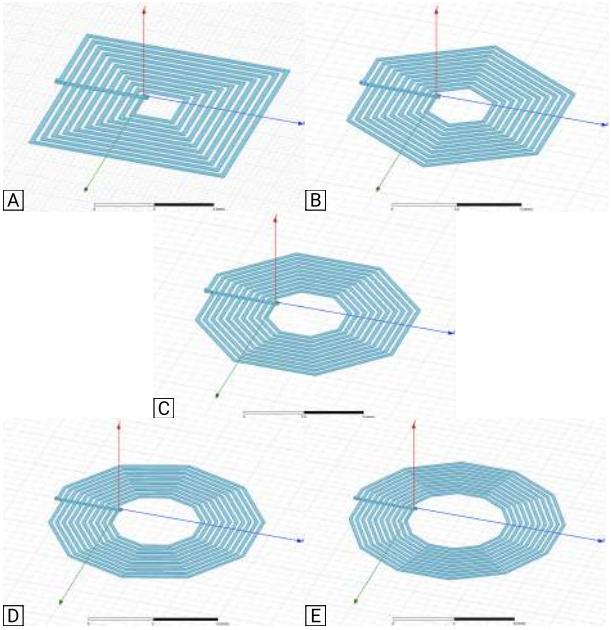

Fig. 4. 1-layer coil layouts simulated in Ansys Software. Segments per turn: A: 4; B: 6; C: 8; D: 10; E: 12.

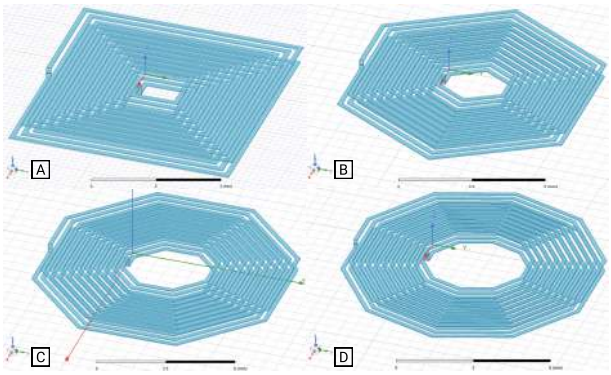

Fig. 5. 2-layer coil layouts simulated in Ansys Software. Segments per turn: A: 4; B: 6; C: 8; D: 10.

adaptive setup was configured with a percent error of 1%, and a minimum of 2 convergence steps.

Regarding the mesh parameters, the type selected for the simulation cases under analysis here was the surface approximation based, for both the coil and the air-box. Around the coil and the coil itself, it was assigned a finer mesh (e.g. Fig. 8B), since this is the critical area for the calculation of self-inductance, while for the air-box a coarser mesh was used (e.g. Fig. 8A).

In Fig. 9 and 10, the self-inductance results for the different 1-layer coil layouts (see Fig. $4A - E$) calculated using the different models are shown. Fig. 9 presents inductance values for coils with 4 and 10 turns, with an inner segment of 0.3mm, and space between turns and wire's width of 0.15mm. Considering the FEM results as the reference, the set of results shown in Fig. 9 show that the range of errors in results from the Modified Wheeler method ranges from 0.99% to 12.67%, and from 2.93% to 9.39% using the Current Sheet Approximation

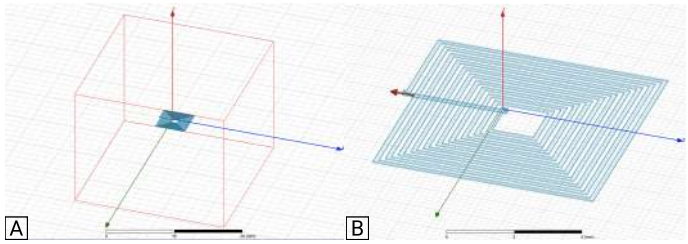

Fig. 6. A: Ansys project with 1-layer coil and air box. B: Current applied into the coil.

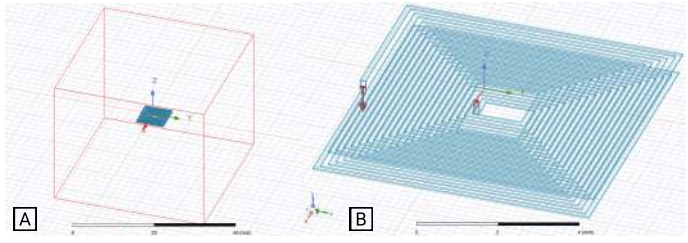

Fig. 7. A: Ansys project with 2-layer coil and air box. B: Current applied into the coil.

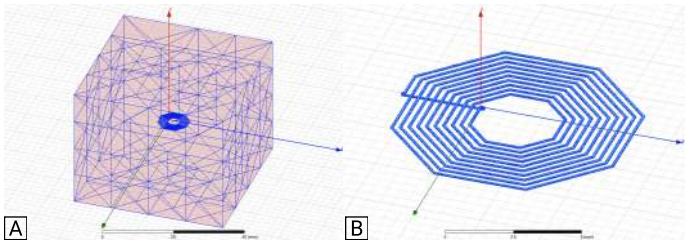

Fig. 8. A: Air box's mesh. B: Coil's mesh.

method. The error registered with the Data Fitted Monomial is from 2.08% to 9.31%, and from 2.13% to 7.93% using the proposed model. In the remaining coil variations (coils with 10 and 12 segments per turn), the proposed model shows errors between 1.39% and 2.45%. Fig. 10 details the data from coils with 4 and 10 turns, with an inner segment of 1.3mm, and with two combinations of the space between turns (s) and the wire's width w, $w = s = 0.10$mm and $w = s = 0.15$mm. Through querying the graphs it is possible to verify that the Modified Wheeler method, for N4 has an error range of $[0.35\% - 15.04\%]$, and for N10 of $[0.18\% - 35.85\%]$. In its turn, the Current Sheet Approximation method has an error range of $[1.45\% - 6.74\%]$ for N4 and $[0.04\% - 6.31\%]$ for N10, while the Data Fitted Monomial shows $[0.69\% - 11.31\%]$ for N4 and $[0.55\% - 3.51\%]$ for N10. With regard to the model proposed in this work, for the case of coils with 4 turns the errors are between 0.06% and 5.90%, and for 10 turns between 0.78% and 2.47%. Particularly, if the 10 and 12 segment coil geometries are considered, the error range drops to values between 0.59% and $3,99\%$ for N4, and 0.62% and $0,79\%$ for N10. Given that, it is possible to see that the errors of the proposed model are at the same level as the error range from the generic formulas, with the advantage of not showing any geometry related limitation, and presenting lower error rangers than some of the approximated expressions.

The same validation procedure has been used for the 2-

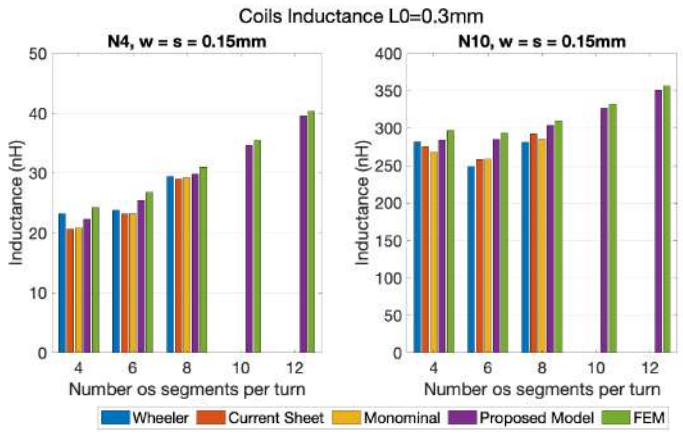

Fig. 9. Comparison between several methods of inductance calculation of coils with 4 and 10 turns, for $L_0 = 0.3mm$, $w = s = 0.10mm$, and for 4, 6, 8, 10, and 12 segments per turn.

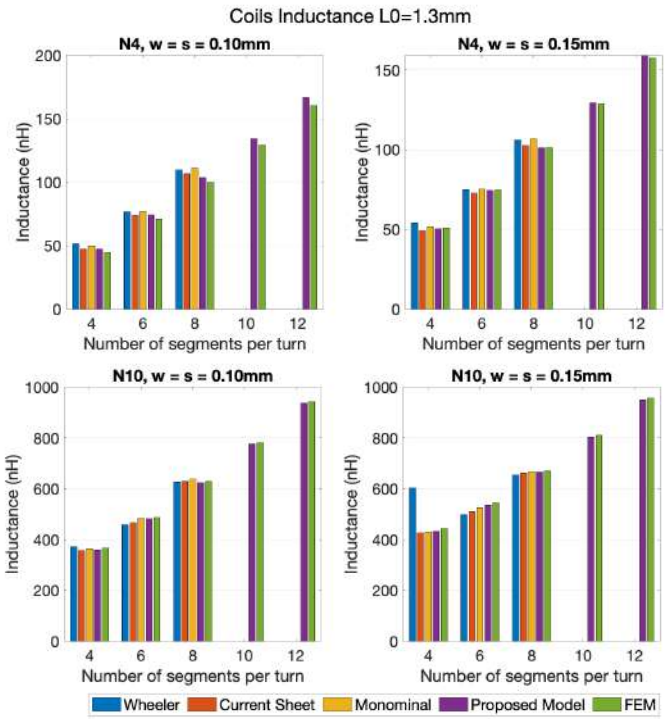

Fig. 10. Comparison between several methods of inductance calculation of coils with 8 and 10 turns, for $L_0 = 1.3mm$, $w = s = 0.10mm$ and $w = s = 0.15mm$, and for 4, 6, 8, 10, and 12 segments per turn.

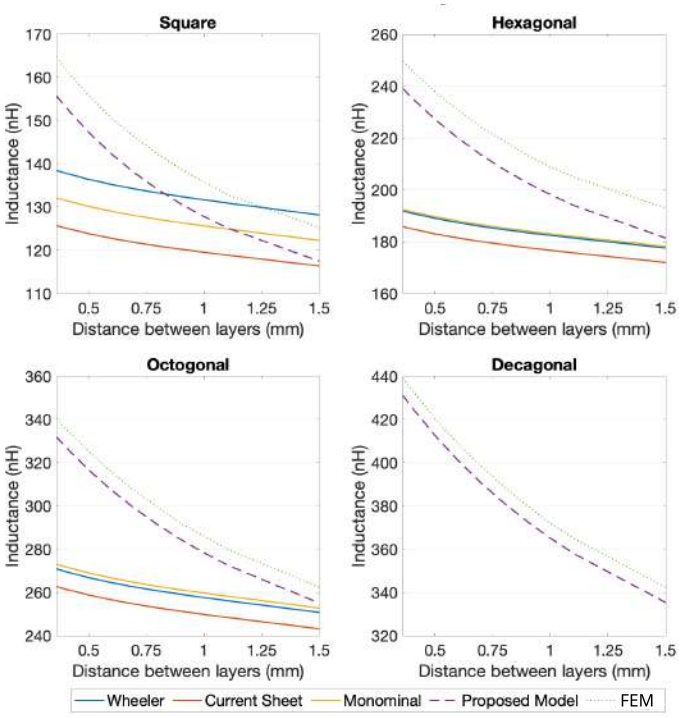

Fig. 11. Comparison between several methods of inductance calculation of 2-layer coils with 4 turns, for $L_0 = 1.3mm$, $w = s = 0.15mm$, and for 4, 6, 8, and 10 segments per turn.

layers planar coils. Considering that, and in order be able to calculate the self-inductance of multi-layer coils using the generic expressions, an additional calculation had to be performed (for the coupling coefficient between the different layers) [20], [21]. Based on that, and looking at the results from Fig.11 and 12, it is noticeable that the proposed model retrieves a much more accurate calculation, when compared to the generic expressions. In view of the results obtained for the 10 turns 2-layer coils, Figure12, the generic expression showed a better performance than for the 4 turns 2-layer ones, (Fig.11, with errors as high as 4.42% for the square geometry, 10.83% for the hexagonal and 6.57% for the octagonal, if the distance between coils is limited to a range of 0.75mm to 2mm (limitation of the coupling coefficient calculation for the generic expressions). For the same selected cases, the proposed model shows maximum errors of 3.53% for the square coils, 2.22% for the hexagonal, 1.56% for the octagonal, and 1.23% for the decagonal.

In view of the results, it can be concluded that, even within the range in which the generic expressions coupling coefficient calculation can be applied, the results obtained using the proposed model are significantly better, with small differences to the outcome of the FEM simulation. Additionally, if the strict geometry limitations of the generic expressions and the coupling coefficient calculation is taken into consideration, it can easily be stated that the developed model is capable of joining reliable results to a versatile calculation method.

B. Experimental Validation

In order to have a complete validation of the proposed model, experimental measurements of self-inductance were performed of several coil configurations. For this experiment, the minimum line width (w) and spacing (s) used in the test coils were of $0.15mm$, due to PCB manufacturer limitations. Fig. 13A shows the PCB produced with the different 1-layer coils namely 4, 6, 8, and 10 segments per turn, with an inner segment of $1.3mm$. These coils were grouped in two sets, one with 10 turns (on the top line) and another with 8 turns (on the bottom line). In each line and for each geometry, there is a pair of coils, one with $w = s = 0.15mm$, and another one with $w = 0.15mm$ and $s = 0.20mm$. In Fig. 13B the 2-layer coils are visible, showing the different geometries of 4, 6, 8, and 10 segments per turn, with an inner segment of $1.3mm$. For the 2-layer coil, only coils with 10 turns were fabricated. The distance between each coil has been chosen in a way that the space is maximized, without creating any effect in the single coil measurement. This was confirmed by comparing the results of a single coil board with the multi-coil measurement setup, without detecting major differences. To minimize any error in the measurement setup, as well as in the coil manufacturing process, two sets of PCBs were produced and the self-inductances in both of them were measured thirteen times. The Keysight Technologies $E4980AL - 102$ LCR precision meter, was used for the inductance measurements at the test frequency of 1MHz, with a four-wire set-up. In order to reduce the measurement noise, the measurement setup visible in Fig.

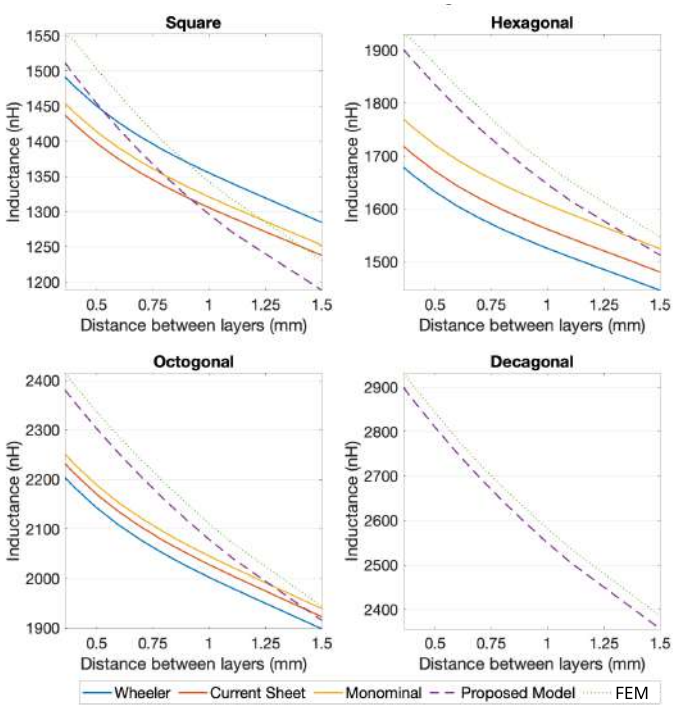

Fig. 12. Comparison between several methods of inductance calculation of 2-layer coils with 10 turns, for $L_0 = 1.3mm$, $w = s = 0.15mm$, and for 4, 6, 8, and 10 segments per turn.

13B was developed to plug the PCB inductances, after the calibration process (Fig. 14).

To compare the experimental measurement of the fabricated coils with the FEM model used as reference here, the thirteen LCR measurements were averaged. During the experimental evaluation process, the maximum deviation registered in both PCBs was around 0.68% for the 1-layer coils, and 0.48%

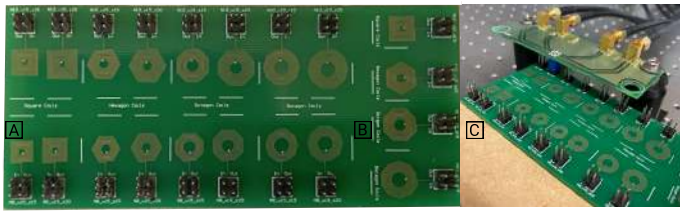

Fig. 13. Measurement Setup.

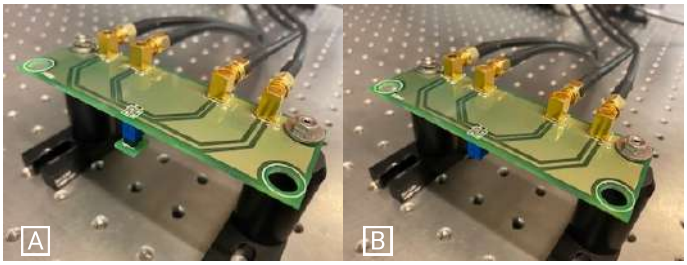

Fig. 14. Calibration Setup. A: Short-Circuit. B: Open-Circuit.

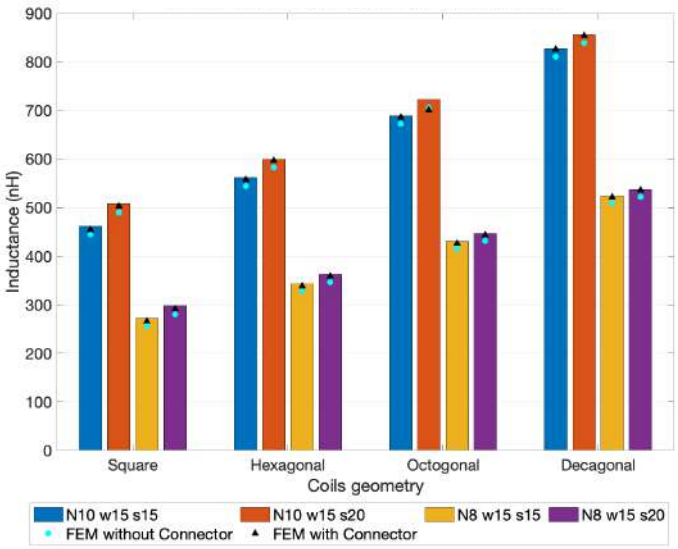

Fig. 15. Graphic with the average inductance values from the experimental measurements and FEM simulation results.

for the 2-layer coils, which proves the high precision of the measurements. The results for the 1-layer coil designs are shown in Fig. 15.

In Fig. 13A, it is noticeable that to perform the measurements, two traces were added to the printed coils, from the coil's extremities until the connectors. For this reason, it was expected that the inductance values measured with the LCR were higher than the ones obtained from the model, and the FEM simulations presented before (as it only considered the coil element). In order to understand the impact and quantify this effect, a FEM model was made with two connecting traces coming out the coil towards the air box.

As predicted, when considering the connecting traces, higher inductance is registered and the error to the experimental measurement is minimized. Comparing the data for single layer coil's from FEM model , one can observe that considering the connecting wires leads to an error reduction of around 2% for $N = 10$, and 3% for $N = 8$.

Finally, the results calculated by the proposed model were compared with experimental measurements, as presented in Fig. 16 and 17. It was also added to the representation the errors of the FEM models with and without connectors, always using the experimental measurement as reference. Note that the coils layouts simulated with our model do not include the extended connecting traces (see Fig. 4 and 5). Comparing the errors of the FEM model without connectors and the ones from the proposed model, it is perceptible that the major contribution to the registered errors is from the absence of the connecting traces in the analysis. Even with this geometry difference, the errors between the experimental measurements and the ones from the proposed model remain acceptable, being in the case of the 1-layer coils smaller than 9% for square coils, 6% for hexagonal, 5% for octagonal, and 4% for decagonal. In the case of 2-layer coils, it is further minimized

to values smaller than 5% for square coils, 3% for hexagonal, 2.5% for octagonal, and 2% for decagonal. It can thus be concluded that the proposed model is valid and has good accuracy for both 1 and 2-layer coils induction calculation.

IV. Conclusions

A versatile, fast, and comprehensive tool to estimate the self-inductance of the planar coil is proposed and validated in this paper. The model was validated by comparison with generic analytical expressions, FEM simulations, and experimental measurements. The results of the model for the different coil geometries show errors, when compared to experimental measurements, always below 10% in the case of the 1-layer coils, and below 5% in the 2-layer coils. In the case of the 1-layer coils, these errors can be considerably decreased if the coil's layout used in the analytical analysis with the proposed model considered the filaments to the measurement connectors, as in the fabricated PCB based coils experimentally used. This tool can be further explored to calculate in fast and reliable way the coupling coefficient between coils, without any geometry limitation, as commonly verified in other calculation methods.

Acknowledgment

This work has been supported by FCT – Fundação para a Ciência e Tecnologia with in the R&D Units Project Scope: UIDB/00319/2020 and European Structural and Investment Funds in the FEDER component, through the Operational Competitiveness and Internationalization Programme (COMPETE 2020) [Project nº 037902; Funding Reference: POCI-01-0247-FEDER-037902].

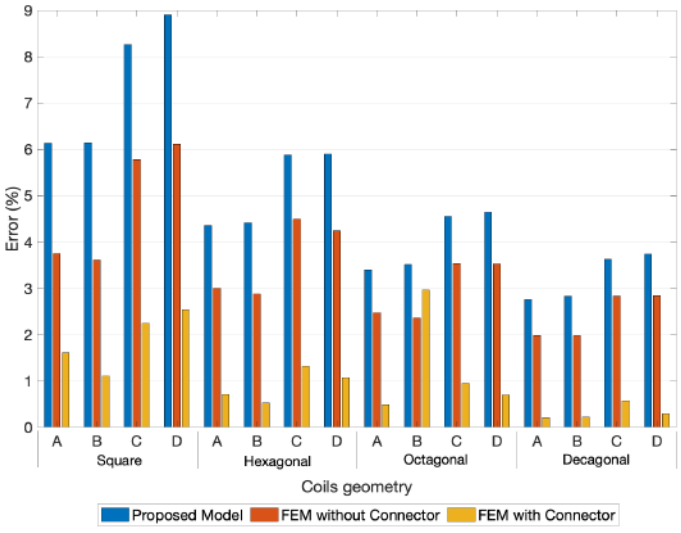

Fig. 16. Errors between the Experimental Measurements, the FEM simulations and the proposed model for the 1-layer coils. A-[$N = 10$, $w = 0.15mm$, and $s = 0.15mm$]; B-[$N = 10$, $w = 0.15mm$, and $s = 0.20mm$]; C-[$N = 8$, $w = 0.15mm$, and $s = 0.15mm$]; D-[$N = 8$, $w = 0.15mm$, and $s = 0.20mm$].

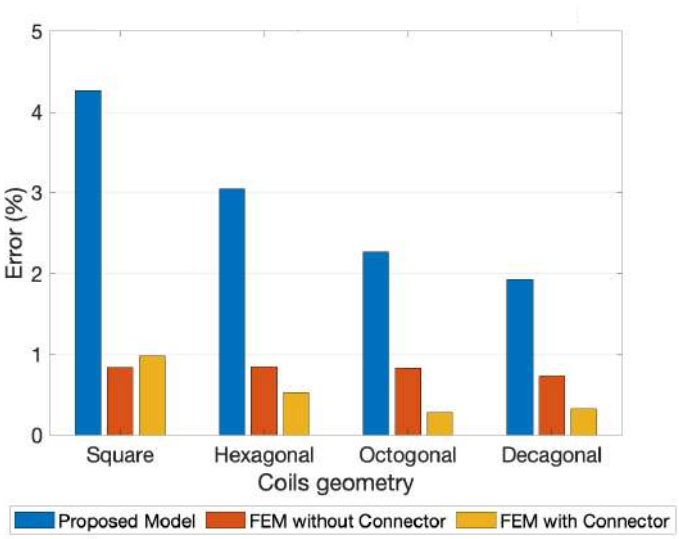

Fig. 17. Errors between the Experimental Measurements, the FEM simulations and the proposed model for the 2-layer coils with 10 turns, $w = s = 0.15mm$, and a $1.3mm$ inner segment.

References

[1] M. Pospisilik, L. Kouril, I. V. O. Motyl, and M. Adamek, "Single and Double Layer Spiral Planar Inductors Optimisation with the Aid of Self-Organising Migrating Algorithm," in *Recent Advances in Signal Processing, Computational Geometry and Systems Theory*, pp. 272–277, 2011.

[2] A. S. A. Kumar, B. George, and S. C. Mukhopadhyay, "Technologies and Applications of Angle Sensors: A Review," *IEEE Sensors Journal*, vol. XX, no. XX, pp. 1–1, 2020.

[3] B. George, Z. Tan, and S. Nihtianov, "Advances in Capacitive, Eddy Current, and Magnetic Displacement Sensors and Corresponding Interfaces," *IEEE Transactions on Industrial Electronics*, vol. 64, pp. 9595–9607, 12 2017.

[4] M. Howard, "Choosing the right position Sensor."

[5] Cambridge Integrated Circuits Ltd, "Resonant Inductive Position Sensors," 2010.

[6] T. Karimov, O. Druzhina, A. Karimov, and D. Butusov, "Axial Movement Sensor Based on Chaotic Oscillator and Planar Coil," *Conference of Open Innovation Association, FRUCT*, vol. 2020-April, pp. 130–135, 2020.

[7] M. Chen, M. Araghchini, K. K. Afridi, J. H. Lang, C. R. Sullivan, and D. J. Perreault, "A Systematic Approach to Modeling Impedances and Current Distribution in Planar Magnetics," *IEEE Transactions on Power Electronics*, vol. 31, pp. 560–580, 1 2016.

[8] N. Lazarus, C. D. Meyer, S. S. Bedair, H. Nochetto, and I. M. Kierzewski, "Multilayer liquid metal stretchable inductors," *Smart Materials and Structures*, vol. 23, no. 8, 2014.

[9] S. R. Khan, S. K. Pavuluri, G. Cummins, and M. P. Desmulliez, "Wireless power transfer techniques for implantable medical devices: A review," *Sensors (Switzerland)*, vol. 20, no. 12, pp. 1–58, 2020.

[10] F. J. Lopez-Alcolea, J. V. D. Real, P. Roncero-Sanchez, and A. P. Torres, "Modeling of a Magnetic Coupler Based on Single- And Double-Layered Rectangular Planar Coils with In-Plane Misalignment for Wireless Power Transfer," *IEEE Transactions on Power Electronics*, vol. 35, no. 5, pp. 5102–5121, 2020.

[11] Q. Wang, M. A. Saket, A. Troy, and M. Ordonez, "A Self-Compensated Planar Coil for Resonant Wireless Power Transfer Systems," *IEEE Transactions on Power Electronics*, vol. 36, no. 1, pp. 674–682, 2021.

[12] V. Cirimele, M. Diana, F. Freschi, and M. Mitolo, "Inductive Power Transfer for Automotive Applications: State-of-the-Art and Future Trends," *IEEE Transactions on Industry Applications*, vol. 54, no. 5, pp. 4069–4079, 2018.

[13] M. Manoufali, K. Bialkowski, B. J. Mohammed, P. C. Mills, and A. Abbosh, "Near-field inductive-coupling link to power a three-dimensional millimeter-size antenna for brain implantable medical devices," *IEEE Transactions on Biomedical Engineering*, vol. 65, no. 1, pp. 4–14, 2018.

[14] B. P. Reddy, A. Murali, and G. Shaga, "Low cost planar coil structure for inductive sensors to measure absolute angular position," in *2017 2nd International Conference on Frontiers of Sensors Technologies (ICFST)*, pp. 14–18, IEEE, 4 2017.

[15] A. S. Anil Kumar, B. George, and S. C. Mukhopadhyay, "An eddy current based non-contact displacement sensor," *I2MTC 2020 - International Instrumentation and Measurement Technology Conference, Proceedings*, pp. 1–6, 2020.

[16] Renesas, "IPS2200 INDUCTIVE POSITION SENSORS A New Era in Motor Commutation," tech. rep., Renesas.

[17] H. Tavakkoli, E. Abbaspour-Sani, A. Khalilzadegan, A. M. Abazari, and G. Rezazadeh, "Mutual inductance calculation between two coaxial planar spiral coils with an arbitrary number of sides," *Microelectronics Journal*, vol. 85, no. December 2018, pp. 98–108, 2019.

[18] B. J. Fletcher, S. Das, and T. Mak, "Design and optimization of inductive-coupling links for 3-D-ICs," *IEEE Transactions on Very Large Scale Integration (VLSI) Systems*, vol. 27, no. 3, pp. 711–723, 2019.

[19] B. J. Fletcher, S. Das, and T. Mak, "A high-speed design methodology for inductive coupling links in 3D-ICs," *Proceedings of the 2018 Design, Automation and Test in Europe Conference and Exhibition, DATE 2018*, vol. 2018-Janua, pp. 497–502, 2018.

[20] J. Zhao, "A new calculation for designing multilayer planar spiral inductors," *Edn*, vol. 55, no. 14, pp. 37–40, 2010.

[21] A. Nejadpak, M. R. Barzegaran, A. Sarikhani, and O. A. Mohammed, "Design of planar inductor based Z-source inverter for residential alternate energy sources," *Conference Proceedings - IEEE Applied Power Electronics Conference and Exposition - APEC*, pp. 1698–1703, 2011.

[22] C. Pacurar, V. Topa, C. Munteanu, A. Racasan, and C. Hebedean, "Spiral inductors inductance computation and layout optimization," *EPE 2012 - Proceedings of the 2012 International Conference and Exposition on Electrical and Power Engineering*, no. Epe, pp. 699–704, 2012.

[23] J. M. Lopez-Villegas, N. Vidal, and J. A. Del Alamo, "Optimized toroidal inductors versus planar spiral inductors in multilayered technologies," *IEEE Transactions on Microwave Theory and Techniques*, vol. 65, no. 2, pp. 423–431, 2017.

[24] M. Ulvr, "Design of PCB search coils for AC magnetic flux density measurement," *AIP Advances*, vol. 8, no. 4, 2018.

[25] C. Pacurar, V. Topa, A. Giurgiuman, C. Munteanu, C. Constantinescu, M. Gliga, and S. Andreica, "The Construction of a Wireless Power Supply System using Planar Spiral Inductors," *Proceedings of 2019 8th International Conference on Modern Power Systems, MPS 2019*, pp. 1–6, 2019.

[26] S. Musunuri and P. Chapman, "Multi-layer spiral inductor design for monolithic DC-DC converters," in *38th IAS Annual Meeting on Conference Record of the Industry Applications Conference, 2003.*, vol. 2, pp. 1270–1275, IEEE, 2003.

[27] J. N. Snyder and F. C. Grover, *Inductance Calculations Working Formulas and Tables*, vol. 18. 1964.

[28] H. Greenhouse, "Design of Planar Rectangular Microelectronic Inductors," *IEEE Transactions on Parts, Hybrids, and Packaging*, vol. 10, pp. 101–109, 6 1974.

[29] S. S. Mohan, M. D. M. Hershenson, S. P. Boyd, and T. H. Lee, "Simple accurate expressions for planar spiral inductances," *IEEE Journal of Solid-State Circuits*, vol. 34, no. 10, pp. 1419–1424, 1999.